Finite Elements in Analysis and Design 51 (2012) 67–80

Contents lists available at SciVerse ScienceDirect

Finite Elements in Analysis and Design

journal homepage: www.elsevier.com/locate/finel

Higher-order linked interpolation in quadrilateral thick plate finite elements

Dragan Ribarić, Gordan Jelenić *

University of Rijeka, Faculty of Civil Engineering, V.C. Emina 5, 51000 Rijeka, Republic of Croatia

ARTICLE INFO

Article history:
Received 22 January 2011
Received in revised form
30 September 2011
Accepted 22 October 2011
Available online 17 December 2011

Keywords:
Finite element method
Mindlin plate theory
Linked interpolation
Higher-order elements

ABSTRACT

In this work, the use of higher-order linked interpolation in the design of plate finite elements is analysed. Benefits of the linked interpolation are well known in the Timoshenko (thick) beam finite elements and in this paper the basis for development of higher-order Mindlin plate elements is found in the analogy between the Timoshenko beam theory and the Mindlin plate theory. The results obtained on standard test examples are compared and numerically assessed against the reference results from literature using various mesh densities and various order of interpolation.

1. Introduction

Many finite elements have been developed for the Mindlin moderately thick plates, and in a number of them the idea of linking the displacement field to the rotations of the cross-sections has been thoroughly investigated and exploited [1–16]. As a general conclusion, it has been realised that this idea on its own cannot eliminate the problem of shear locking, especially for coarse meshes, which is in stark contrast to the results obtained by applying the idea to the Timoshenko beam elements [7,17–23]. Consequently, a number of remedies have been proposed, which are mostly based on using adjusted material parameters [24] or on the application of the assumed strain [2,14,15] or the enhanced strain [25] concepts or the use of mixed approaches [1,3,6,11,12] or hybrid approaches [9].

In this paper, we re-visit this classic topic and study the possibility of eliminating the shear-locking problem while remaining firmly in the framework of the standard displacement-based finite-element design technique. Within this approach, the kinematic and constitutive equations of the problem are satisfied in the strong sense, while the equilibrium equations are satisfied in the weak sense with the unknown displacement and rotation fields as the only interpolated quantities. In contrast to most of the existing displacement-based approaches, which base their developments on constraining the shape functions for the displacement and the rotation fields so as to produce a required distribution of the shear strains [8,10,24,26], here we extend the higher-order linked interpolation functions developed for the Timoshenko beam to the plate structures and investigate the results and their relationships with the known approaches.

In Section 2, we illustrate the relevant results for the Timoshenko beam elements from [18] giving a family of interpolation functions which follow a very structured pattern and provide the exact solution for arbitrary polynomial loadings. In some sense, the Mindlin theory of thick plates may be regarded as a 2D generalisation of the Timoshenko theory of thick beams. In stark contrast to thick beams, however, the differential equations of equilibrium for thick plates cannot be solved in terms of a finite number of parameters and consequently no exact finite-element interpolation can be found in this way. Nonetheless, in [1,3,27] such interpolation has been used to formulate three-node triangular and four-node quadrilateral thick plate elements, while in [2,6] a six-node triangular and an eight-node quadrilateral elements have been proposed.

In Section 3, we firstly consider a quadrilateral four-node plate element, for which the constant shear strain condition imposed on the element edges is known to lead to an interpolation for the displacement field which is dependent not only on the nodal displacements, but also on the nodal rotations around the in-plane normal directions to the element edges. In this way, the displacement interpolation becomes linked to the nodal rotations via shape functions which are linear in one direction and quadratic in the other. Such linked interpolation for plates may be also obtained as a 2D generalisation of the linked interpolation for beams [18]. This approach enables an easy generalisation of the linked-interpolation concept to higher-order rectangular plate elements. A different approach to achieve a similar goal has been pursued in [8] where a family of displacement-based

* Corresponding author. Tel.: +385 51 352 114; fax: +385 51 332 816.
E-mail address: gordan@gradri.hr (G. Jelenić).

0168-874X/$ - see front matter © 2011 Elsevier B.V. All rights reserved.
doi:10.1016/j.finel.2011.10.003

linked-interpolation triangular elements has been derived on a premise of the shear strain variation being of a prescribed order. Secondly, we note that generalising this idea to arbitrary quadrilateral shapes is non-trivial and special care needs to be taken for such elements to satisfy the standard patch tests. We present a manner in which quadrilateral elements may be properly developed, which involves an additional internal displacement degree of freedom as in [26]. Finally, we conduct some numerical tests which demonstrate the potential of this approach, in particular for the higher-order elements.

2. Exact solution of Timoshenko beam problem for polynomial loading

In the Timoshenko beam theory, the initial planar cross section of a beam remains planar after the deformation, but the angle which it closes with the centroidal axis may change during the deformation resulting in the shear angle

$$\gamma = \frac{dw}{dx} - (-\theta) = w' + \theta,$$

where w is the lateral displacement of the beam shown in Fig. 1, the dash ($'$) indicates a differentiation with respect to the co-ordinate x, and θ is the rotation of a cross section.

Let us also define the linear-elastic constitutive equations as $M = EI\theta'$ and $S = GA_s\gamma$, where M and S are the cross-sectional stress-couple and shear stress resultants, while EI and GA_s are the bending and shear stiffness, respectively, as well as the equilibrium equations $M' = S$ and $S' = -q$, where q is the distributed loading per unit of length of the beam. This results in the following differential equations of the Timoshenko beam:

$$EI\theta''' = -q, \quad GA_s(w'' + \theta') = -q$$

having the following general solution for a polynomial loading q of order $n-4$ [18]:

$$\theta = \sum_{i=1}^{n} I_i\theta_i, \quad w = \sum_{i=1}^{n} I_i w_i - \frac{L}{n}\prod_{j=1}^{n} N_j \sum_{i=1}^{n} (-1)^{i-1}\binom{n-1}{i-1}\theta_i, \tag{1}$$

where L is the beam length, θ_i and w_i are the values of the displacements and the rotations at the n nodes equidistantly spaced between the beam ends, I_i are the standard Lagrangian polynomials of order $n-1$, and $N_j = x/L$ for $j=1$ and $N_j = 1-(n-1)/(j-1)(x/L)$ otherwise. In the natural co-ordinate system with $\xi = (2x/L)-1$ the displacement solution reads

$$w = \sum_{i=1}^{n} I_i w_i - \frac{L}{n}\sum_{i=1}^{n} \frac{\xi - \xi_i}{2} I_i\theta_i.$$

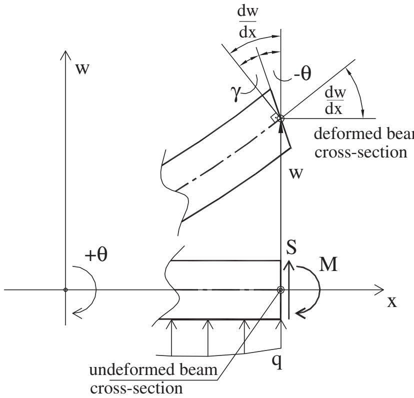

Fig. 1. Initial and deformed configuration of a moderately thick beam.

3. Family of linked-interpolation elements for Mindlin plates

The Mindlin plate theory may be regarded as a generalisation of the Timoshenko beam theory to two-dimensional structures. The plate analysed is assumed to be of a uniform thickness h with a mid-surface lying in the horizontal co-ordinate plane and a distributed loading q assumed to act on the plate mid-surface in the direction perpendicular to it. The angles which the vertical material line elements close with the mid-surface are not necessarily retained during the deformation process, which results in the following shear angles and curvature expressions [3]:

$$\boldsymbol{\Gamma} = \begin{Bmatrix} \gamma_{xz} \\ \gamma_{yz} \end{Bmatrix} = \begin{Bmatrix} \theta_y + \frac{\partial w}{\partial x} \\ -\theta_x + \frac{\partial w}{\partial y} \end{Bmatrix} = \begin{bmatrix} 0 & 1 \\ -1 & 0 \end{bmatrix}\begin{Bmatrix} \theta_x \\ \theta_y \end{Bmatrix} + \begin{Bmatrix} \frac{\partial}{\partial x} \\ \frac{\partial}{\partial y} \end{Bmatrix} w = \mathbf{e}\boldsymbol{\theta} + \nabla w, \tag{2}$$

$$\boldsymbol{\kappa} = \begin{Bmatrix} \kappa_x \\ \kappa_y \\ \kappa_{xy} \end{Bmatrix} = \begin{Bmatrix} \frac{\partial \theta_y}{\partial x} \\ -\frac{\partial \theta_x}{\partial y} \\ \frac{\partial \theta_y}{\partial y} - \frac{\partial \theta_x}{\partial x} \end{Bmatrix} = \begin{bmatrix} 0 & \frac{\partial}{\partial x} \\ -\frac{\partial}{\partial y} & 0 \\ -\frac{\partial}{\partial x} & \frac{\partial}{\partial y} \end{bmatrix}\begin{Bmatrix} \theta_x \\ \theta_y \end{Bmatrix} = \mathbf{L}\boldsymbol{\theta}, \tag{3}$$

where $\boldsymbol{\theta}$ is the rotation vector with components θ_x and θ_y around the respective horizontal global co-ordinate axes, w is the transverse displacement field, $\boldsymbol{\Gamma}$ is the shear strain vector and $\boldsymbol{\kappa}$ is the curvature vector. ∇w is a gradient on the displacement field and $\mathbf{L}$ is a differential operator on the rotation field. Here, we shall be using the constitutive equations for a linear elastic material

$$\mathbf{M} = \begin{Bmatrix} M_x \\ M_y \\ M_{xy} \end{Bmatrix} = \frac{Eh^3}{12(1-\nu^2)}\begin{bmatrix} 1 & \nu & 0 \\ \nu & 1 & 0 \\ 0 & 0 & \frac{1-\nu}{2} \end{bmatrix}\begin{Bmatrix} \frac{\partial \theta_y}{\partial x} \\ -\frac{\partial \theta_x}{\partial y} \\ \frac{\partial \theta_y}{\partial y} - \frac{\partial \theta_x}{\partial x} \end{Bmatrix} = \mathbf{D_b}\boldsymbol{\kappa} = \mathbf{D_b}\mathbf{L}\boldsymbol{\theta}$$

$$\mathbf{S} = \begin{Bmatrix} S_x \\ S_y \end{Bmatrix} = kGh\begin{bmatrix} 1 & 0 \\ 0 & 1 \end{bmatrix}\begin{Bmatrix} \gamma_{xz} \\ \gamma_{yz} \end{Bmatrix} = \mathbf{D_s}\boldsymbol{\Gamma} = \mathbf{D_s}(\mathbf{e}\boldsymbol{\theta} + \nabla w), \tag{4}$$

where M_x, M_y, and M_{xy} are the bending and twisting moments around the respective co-ordinate axes, S_x and S_y are the shear-stress resultants, E and G are the Young and shear moduli, while ν and k are Poisson's coefficient and the shear correction factor usually set to 5/6. The differential equations of equilibrium are given as

$$\frac{\partial M_x}{\partial x} + \frac{\partial M_{xy}}{\partial y} = S_x, \quad \frac{\partial M_{xy}}{\partial x} + \frac{\partial M_y}{\partial y} = S_y, \quad \frac{\partial S_x}{\partial x} + \frac{\partial S_y}{\partial y} = -q, \tag{5}$$

where q is now the distributed loading per unit area of the plate and normal to it. The above results in differential equations of the linear elastic Mindlin plate which, in contrast to the earlier Timoshenko beam case, cannot be solved in terms of a finite number of parameters, hence the finite-element solution cannot give the exact result. However, an idea to extend the results from Section 2 to the plate case is still attractive as a design tool to derive more accurate Mindlin plate elements. Instead of the differential equations of equilibrium from (5) they are derived from the functional of the total potential energy

$$\begin{aligned} \Pi(w,\theta_x,\theta_y) &= \frac{1}{2}\int(\mathbf{M}^T\boldsymbol{\kappa})dA + \frac{1}{2}\int(\mathbf{S}^T\boldsymbol{\Gamma})dA + \Pi_{ext} \\ &= \frac{1}{2}\int(\boldsymbol{\kappa}^T\mathbf{D_b}\boldsymbol{\kappa})dA + \frac{1}{2}\int(\boldsymbol{\Gamma}^T\mathbf{D_s}\boldsymbol{\Gamma})dA + \Pi_{ext}, \end{aligned} \tag{6}$$

where the first term is the bending strain energy stored in the system, the second term is the shear strain energy and the third term describes the potential energy of the distributed and boundary loading.

3.1. Linked interpolation for a four-node quadrilateral plate element

The linked interpolation as defined in (1) may be applied to 2D situation in its original form written for arbitrary number of nodal points, but such a form would not be very illustrative. Instead, here we shall first apply it to a quadrilateral element with four nodal points at the element vertices as in [1–3,7,9,11] (see Fig. 2). At each nodal point i (i=1, 2, 3, 4) there exist three degrees of freedom (displacement w_i, and rotations θ_{x_i}, and θ_{y_i}). In analogy to (1), the linked interpolation for the displacement field may be now given as

$$w = I_1 w_1 + I_2 w_2 + I_3 w_3 + I_4 w_4 - \frac{a_1}{2}\,\frac{1-\xi^2}{4}\,\frac{1-\eta}{2}(\theta^1_{na_1}-\theta^2_{na_1}) - \frac{a_2}{2}\,\frac{1-\xi^2}{4}\,\frac{1+\eta}{2}(\theta^4_{na_2}-\theta^3_{na_2}) + \frac{b_1}{2}\,\frac{1-\xi}{2}\frac{1-\eta^2}{4}(\theta^1_{nb_1}-\theta^4_{nb_1}) + \frac{b_2}{2}\,\frac{1+\xi}{2}\,\frac{1-\eta^2}{4}(\theta^2_{nb_2}-\theta^3_{nb_2}), \tag{7}$$

where ξ and η are the standard natural co-ordinates, a_i and b_i (i=1, 2) are the lengths of the element sides as shown in Fig. 2, the Lagrangian shape functions are given as

$$I_1 = \frac{1-\xi}{2}\frac{1-\eta}{2}, \quad I_2 = \frac{1+\xi}{2}\frac{1-\eta}{2}, \quad I_3 = \frac{1+\xi}{2}\frac{1+\eta}{2},$$
$$I_4 = \frac{1-\xi}{2}\,\frac{1+\eta}{2} \quad \text{and} \quad \theta^k_{na_i}, \theta^k_{nb_i}$$

are the rotation components perpendicular to the element side a_i or b_i at node k (see Fig. 3).

The interpolation functions for the rotations are given in a usual manner using the standard Lagrangian polynomials:

$$\theta_x = \sum_{i=1}^{4} I_i \theta_{x_i}, \quad \theta_y = \sum_{i=1}^{4} I_i \theta_{y_i}. \tag{8}$$

All the interpolation functions are expressed in natural coordinates ξ and η, which are related to the Cartesian co-ordinates x and y via $x=\sum_{i=1}^{4} I_i x_i$, $y=\sum_{i=1}^{4} I_i y_i$. The normal rotations about an element edge are shown in Fig. 4 and expressed by the global node rotations as

$$\theta^1_{na_1} = -\theta_{x_1}\frac{y_2-y_1}{a_1} + \theta_{y_1}\frac{x_2-x_1}{a_1} \quad \text{and}$$
$$\theta^1_{na_1} - \theta^2_{na_1} = -(\theta_{x_1}-\theta_{x_2})\frac{y_2-y_1}{a_1} + (\theta_{y_1}-\theta_{y_2})\frac{x_2-x_1}{a_1}.$$

The linked interpolation as employed in a two-node Timoshenko beam element can exactly reproduce the quadratic displacement function, and the same should be expected for the 2D interpolation considered here. However, this must be true for any direction, which interpolation (7) cannot satisfy unless enriched by a bi-quadratic bubble term $(1-\xi^2)/4(1-\eta^2)/4\, w_b$ eventually giving

$$w = w_{eqn(7)} + \frac{1-\xi^2}{4}\,\frac{1-\eta^2}{4} w_b, \tag{9}$$

where $w_{eqn(7)}$ is the displacement interpolation given in (7) and w_b is an internal bubble parameter. The displacement and rotational interpolations (9) and (8) can reproduce a constant bending moment and zero shear distribution throughout the arbitrary quadrilateral element.

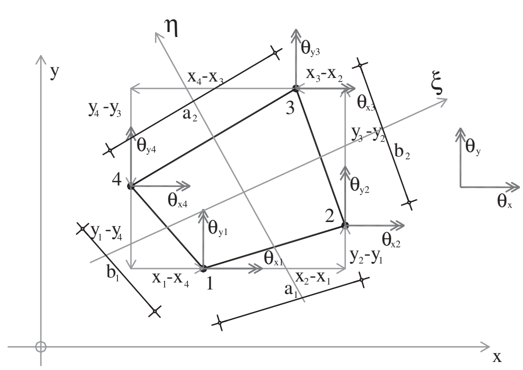

Fig. 2. Four-node quadrilateral plate element and its nodal rotations. The nodal displacements are perpendicular to the element plane.

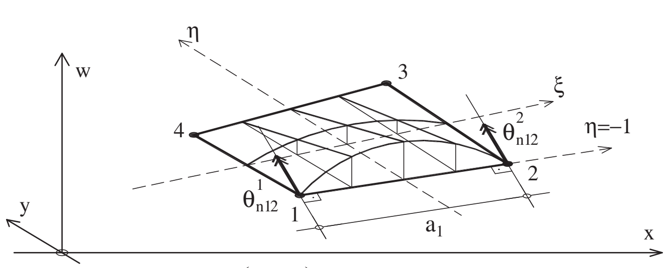

$$-\frac{a_1}{2}\left(\frac{1-\xi^2}{4}\right)\left(\frac{1-\eta}{2}\right)(\theta^1_{na1}-\theta^2_{na1})$$

Fig. 3. Linking shape function for normal rotations on the side "1–2" of the element.

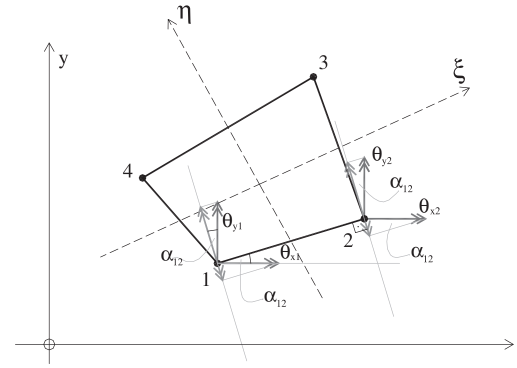

Fig. 4. Components of the nodal rotations to the normal on the side between nodes 1 and 2.

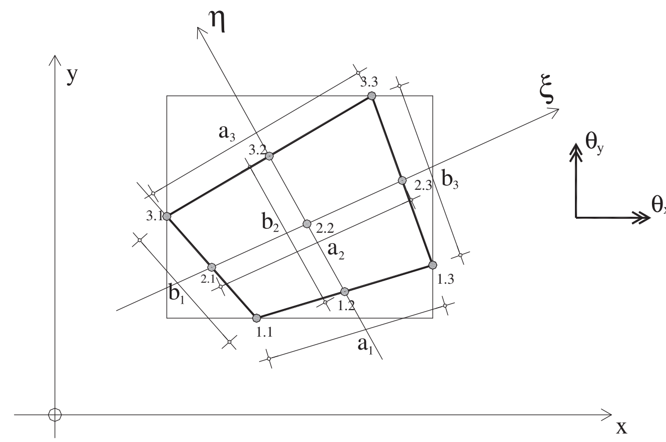

Fig. 5. Nine-node quadrilateral plate element and its geometry.

3.2. Linked interpolation for a nine-node quadrilateral plate element

For a nine-node quadrilateral element the linked interpolation for the displacement field may be defined correspondingly (written in positional order as shown in Fig. 5), i.e.

$$w = I_{1\xi}I_{3\eta}w_{3,1} + I_{2\xi}I_{3\eta}w_{3,2} + I_{3\xi}I_{3\eta}w_{3,3} + I_{1\xi}I_{2\eta}w_{2,1} + I_{2\xi}I_{2\eta}w_{2,2} + I_{3\xi}I_{2\eta}w_{2,3}$$

$$
\begin{aligned}
&+I_{1\xi}I_{1\eta}w_{1,1}+I_{2\xi}I_{1\eta}w_{1,2}+I_{3\xi}I_{1\eta}w_{1,3}\\
&+\frac{a_3}{3}\,\frac{\xi-\xi^3}{4}\,\frac{1+\eta}{2}\,\eta(\theta^{3,1}_{na_3}-2\theta^{3,2}_{na_3}+\theta^{3,3}_{na_3})\\
&+\frac{a_2}{3}\,\frac{\xi-\xi^3}{4}\,4\,\frac{1+\eta}{2}\,\frac{1-\eta}{2}(\theta^{2,1}_{na_2}-2\theta^{2,2}_{na_2}+\theta^{2,3}_{na_2})\\
&-\frac{a_1}{3}\,\frac{\xi-\xi^3}{4}\,\eta\,\frac{1-\eta}{2}(\theta^{1,1}_{na_1}-2\theta^{1,2}_{na_1}+\theta^{1,3}_{na_1})\\
&+\frac{b_1}{3}\,\xi\,\frac{1-\xi}{2}\,\frac{\eta-\eta^3}{4}(\theta^{1,1}_{nb_1}-2\theta^{2,1}_{nb_1}+\theta^{3,1}_{nb_1})\\
&-\frac{b_2}{3}\,4\,\frac{1+\xi}{2}\,\frac{1-\xi}{2}\,\frac{\eta-\eta^3}{4}(\theta^{1,2}_{nb_2}-2\theta^{2,2}_{nb_2}+\theta^{3,2}_{nb_2})\\
&-\frac{b_3}{3}\,\frac{1+\xi}{2}\,\xi\,\frac{\eta-\eta^3}{4}(\theta^{1,3}_{nb_3}-2\theta^{2,3}_{nb_3}+\theta^{3,3}_{nb_3}),
\end{aligned}
\tag{10}
$$

where $I_{1\xi}=-\xi(1-\xi)/2$, $I_{2\xi}=1-\xi^2$, $I_{3\xi}=\xi(1+\xi)/2$, $I_{1\eta}$, $I_{2\eta}$, $I_{3\eta}$ are the corresponding interpolation functions with natural coordinate η, a_k and b_k (k=1, 3) are the node line lengths in ξ and η directions as shown in Fig. 5. Again, $\theta^{i,j}_{na_k}$ and $\theta^{i,j}_{nb_k}$ are the components of the nodal rotations to the normal of the respective element line at node (i, j). This time a node has two indices denoting its position (row and column number counted from the lower left corner node).

The interpolation for the rotation fields, in positional order, reads

$$
\theta_x=\sum_{i=1}^{3}\sum_{j=1}^{3}I_{i\eta}I_{j\xi}\theta_{x_{i,j}},\quad \theta_y=\sum_{i=1}^{3}\sum_{j=1}^{3}I_{i\eta}I_{j\xi}\theta_{y_{i,j}},
\tag{11}
$$

where $\theta_{x_{i,j}}$ and $\theta_{y_{i,j}}$ denote rotations in the global directions at the node denoted as (i, j). The isoparametric mapping from the natural coordinates ξ and η to the global variables x and y follows the standard rule

$$
x=\sum_{i=1}^{3}\sum_{j=1}^{3}I_{i\eta}I_{j\xi}x_{i,j},\quad y=\sum_{i=1}^{3}\sum_{j=1}^{3}I_{i\eta}I_{j\xi}y_{i,j}.
$$

In these expressions, the coordinates for nodes (1,2), (2,3), (3,2) and (2,1) are in the middle between the adjacent nodes and node (2,2) is at the element centroid.

As before, in order to reproduce exactly the polynomial of the third order in arbitrary direction, an additional bi-cubic term involving an internal bubble displacement w_b has to be added to displacement interpolation (10). Eventually, therefore, the displacement interpolation reads

$$
w=w_{eqn(10)}+\frac{\xi-\xi^3}{4}\,\frac{\eta-\eta^3}{4}w_b.
\tag{12}
$$

The displacement and rotational interpolations (12) and (11) can reproduce the states of linear bending throughout the arbitrary quadrilateral element.

A similar interpolation for the displacements has been applied to six-node triangular plate elements in [6], while a serendipity-type formulation of a similar sort written in a framework of the hierarchical interpolation has been presented in [2]. A family of triangular elements based on the linked interpolation has been derived in [8] stemming from the requirement of the shear strain in the element being of a prescribed order. The above methodology, in contrast, generates the linked interpolation from the underlying interpolation functions developed for the beam elements and may be consistently applied to quadrilateral plate elements of arbitrary order.

3.3. *Linked interpolation for a sixteen-node quadrilateral plate element*

A sixteen-node (4 × 4) linked-interpolation quadrilateral element (Fig. 6) may be defined correspondingly.

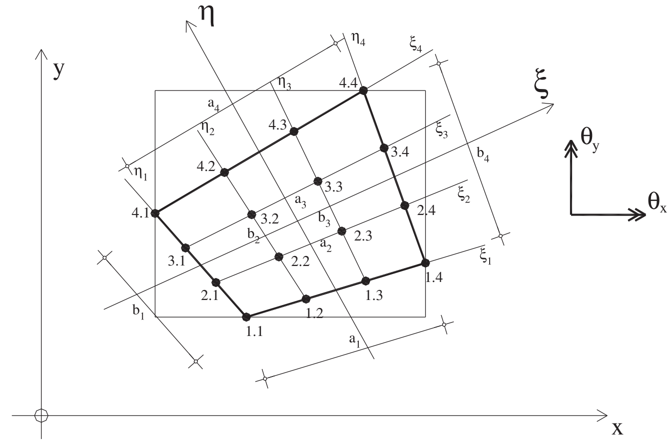

Fig. 6. Sixteen-node quadrilateral plate element and its geometry.

The displacement field is defined as

$$
\begin{aligned}
w=&\sum_{i=1}^{4}\sum_{j=1}^{4}I_{i\eta}I_{j\xi}w_{i,j}+I_{4\eta}\prod_{n=1}^{4}N_{n\xi}\frac{a_4}{4}(\theta^{4,1}_{na_4}-3\theta^{4,2}_{na_4}+3\theta^{4,3}_{na_4}-\theta^{4,4}_{na_4})\\
&+I_{3\eta}\prod_{n=1}^{4}N_{n\xi}\frac{a_3}{4}(\theta^{3,1}_{na_3}-3\theta^{3,2}_{na_3}+3\theta^{3,3}_{na_3}-\theta^{3,4}_{na_3})\\
&+I_{2\eta}\prod_{n=1}^{4}N_{n\xi}\frac{a_2}{4}(\theta^{2,1}_{na_2}-3\theta^{2,2}_{na_2}+3\theta^{2,3}_{na_2}-\theta^{2,4}_{na_2})\\
&+I_{1\eta}\prod_{n=1}^{4}N_{n\xi}\frac{a_1}{4}(\theta^{1,1}_{na_1}-3\theta^{1,2}_{na_1}+3\theta^{1,3}_{na_1}-\theta^{1,4}_{na_1})\\
&+I_{1\xi}\prod_{n=1}^{4}N_{n\eta}\frac{b_1}{3}(\theta^{1,1}_{nb_1}-3\theta^{2,1}_{nb_1}+3\theta^{3,1}_{nb_1}-\theta^{4,1}_{nb_1})\\
&+I_{2\xi}\prod_{n=1}^{4}N_{n\eta}\frac{b_2}{3}(\theta^{1,2}_{nb_2}-3\theta^{2,2}_{nb_2}+3\theta^{3,2}_{nb_2}-\theta^{4,2}_{nb_2})\\
&+I_{3\xi}\prod_{n=1}^{4}N_{n\eta}\frac{b_3}{3}(\theta^{1,3}_{nb_3}-3\theta^{2,3}_{nb_3}+3\theta^{3,3}_{nb_3}-\theta^{4,3}_{nb_3})\\
&+I_{4\xi}\prod_{n=1}^{4}N_{n\eta}\frac{b_4}{3}(\theta^{1,4}_{nb_4}-3\theta^{2,4}_{nb_4}+3\theta^{3,4}_{nb_4}-\theta^{4,4}_{nb_4}),
\end{aligned}
\tag{13}
$$

where

$$
I_{1\xi}=-\frac{9}{16}\left(\xi+\frac{1}{3}\right)\left(\xi-\frac{1}{3}\right)(\xi-1)\qquad I_{1\eta}=-\frac{9}{16}\left(\eta+\frac{1}{3}\right)\left(\eta-\frac{1}{3}\right)(\eta-1)
$$

$$
I_{2\xi}=+\frac{27}{16}(\xi+1)\left(\xi-\frac{1}{3}\right)(\xi-1)\qquad I_{2\eta}=+\frac{27}{16}(\eta-1)\left(\eta-\frac{1}{3}\right)(\eta-1)
$$

$$
I_{3\xi}=-\frac{27}{16}(\xi+1)\left(\xi+\frac{1}{3}\right)(\xi-1)\qquad I_{3\eta}=-\frac{27}{16}(\eta+1)\left(\eta+\frac{1}{3}\right)(\eta-1)
$$

$$
I_{4\xi}=+\frac{9}{16}(\xi+1)\left(\xi+\frac{1}{3}\right)\left(\xi-\frac{1}{3}\right)\qquad I_{4\eta}=+\frac{9}{16}(\eta+1)\left(\eta+\frac{1}{3}\right)\left(\eta-\frac{1}{3}\right)
$$

$$
\prod_{n=1}^{4}N_{n\xi}=-\frac{9}{32}(\xi+1)\left(\xi+\frac{1}{3}\right)\left(\xi-\frac{1}{3}\right)(\xi-1)
$$

$$
\prod_{n=1}^{4}N_{n\eta}=-\frac{9}{32}(\eta+1)\left(\eta+\frac{1}{3}\right)\left(\eta-\frac{1}{3}\right)(\eta-1)
$$

and where $\theta^{i,j}_{na_k}$ and $\theta^{i,j}_{nb_k}$ (k=1, 4) denote the rotation projections normal to the node line lengths a_k or b_k at node (i,j).

The interpolations for the rotation fields, in positional order, read

$$
\theta_x=\sum_{i=1}^{4}\sum_{j=1}^{4}I_{i\eta}I_{j\xi}\theta_{x_{i,j}},\theta_y=\sum_{i=1}^{4}\sum_{j=1}^{4}I_{i\eta}I_{j\xi}\theta_{y_{i,j}},
\tag{14}
$$

where $\theta_{x_{i,j}}$ and $\theta_{y_{i,j}}$ denote the rotations in the global directions at node (i,j) and the isoparametric mapping from natural coordinates ξ and η to global variables x and y follows as:

$$x=\sum_{i=1}^{4}\sum_{j=1}^{4}I_{i\eta}I_{j\xi}x_{i,j},\quad y=\sum_{i=1}^{4}\sum_{j=1}^{4}I_{i\eta}I_{j\xi}y_{i,j}.$$

In these expressions, the coordinates for the nodes along any element side are equally spaced (a third of lengths a_k and b_k) and the internal nodes follow the same rule along their lines in both directions.

Finally, the bubble term completes the displacement interpolation

$$\begin{aligned}w&=w_{eqn(13)}+\frac{9}{32}(\xi^2-1)\left(\xi^2-\frac{1}{9}\right)\frac{9}{32}(\eta^2-1)\left(\eta^2-\frac{1}{9}\right)\cdot w_b\\&=w_{eqn(13)}+\prod_{n=1}^{4}N_n(\xi)\prod_{n=1}^{4}N_n(\eta)\cdot w_b,\end{aligned}\tag{15}$$

3.4. Finite element stiffness matrix and load vector

In general, all interpolations may be written in matrix form as

$$w=\mathbf{I}_{ww}\mathbf{w}+\mathbf{N}_{w\theta}\boldsymbol{\theta}_{x,y}+N_{wb}w_b,\tag{16}$$

$$\begin{Bmatrix}\theta_x\\\theta_y\end{Bmatrix}=\mathbf{I}_{\theta\theta}\boldsymbol{\theta}_{x,y},\tag{17}$$

where $\mathbf{I}_{ww}$ is a matrix of all interpolation functions concerning nodal displacement parameters of the form $I_{i\eta}I_{j\xi}$ with the dimension $1\times N_{\rm nd}$ ($N_{\rm nd}=n^2$, n is the number of nodes per element side) and $\mathbf{w}$ is a vector of nodal displacement parameters with the dimension $N_{\rm nd}$: $\mathbf{w}^T=\langle w_{1,1}\ldots w_{n,n}\rangle$, $\mathbf{N}_{w\theta}$ is a matrix of all linked interpolation functions projected to global coordinate directions x and y with the dimension $1\times 2N_{\rm nd}$ and $\boldsymbol{\theta}_{x,y}$ is a vector of nodal rotations in global coordinate directions with the dimension $2N_{\rm nd}$: $\boldsymbol{\theta}^T_{x,y}=\langle\theta_{x1,1},\theta_{y1,1}\ldots\theta_{xn,n},\theta_{yn,n}\rangle$, N_{wb} is a bubble interpolation function in (9), (12) or (15) and w_b is the bubble parameter. $\mathbf{I}_{\theta\theta}$ is again a matrix of all interpolation functions concerning rotational parameters described in (8), (11) or (14) and has the dimension $2\times 2N_{\rm nd}$.

The formation of the element stiffness matrix and the external load vector for the interpolation functions defined in this way follows the standard finite-element procedure described in textbooks e.g. [28–30]. A functional of the total energy of the system is expressed as (6) and from the stationarity condition for the total potential energy functional over an element, a system of algebraic equations is derived

$$\begin{bmatrix}\mathbf{K}_{\mathbf{S}ww}&\mathbf{K}^T_{\mathbf{S}w\theta}&\mathbf{K}^T_{\mathbf{S}wb}\\\mathbf{K}_{\mathbf{S}w\theta}&\mathbf{K}_{\mathbf{B}\theta\theta}+\mathbf{K}_{\mathbf{S}\theta\theta}&\mathbf{K}^T_{\mathbf{S}b\theta}\\\mathbf{K}_{\mathbf{S}wb}&\mathbf{K}_{\mathbf{S}b\theta}&k_{\mathbf{S}bb}\end{bmatrix}\begin{bmatrix}\mathbf{w}\\\boldsymbol{\theta}_{x,y}\\w_b\end{bmatrix}=\begin{bmatrix}\mathbf{f}_w\\\mathbf{f}_\theta\\f_b\end{bmatrix},$$

where vectors $\mathbf{f}_w$, $\mathbf{f}_\theta$ and scalar f_b are the terms due to external loading. Of all the parts of the stiffness matrix only one depends on the bending strain energy

$$\mathbf{K}_{\mathbf{B}\theta\theta}=\int_A(\mathbf{L}\mathbf{I}_{\theta\theta})^T\mathbf{D_b}(\mathbf{L}\mathbf{I}_{\theta\theta})dA$$

and is calculated from interpolation functions for rotations θ_x and θ_y. This square block has the dimension of two times the number of element nodes. All other blocks are derived from the shear strain energy:

$$\mathbf{K}_{\mathbf{S}ww}=\int_A(\nabla\mathbf{I}_{ww})^T\mathbf{D_s}(\nabla\mathbf{I}_{ww})dA$$

$$k_{\mathbf{S}bb}=\int_A(\nabla N_{wb})^T\mathbf{D_s}(\nabla N_{wb})dA$$

$$\mathbf{K}_{\mathbf{S}\theta\theta}=\int_A(\mathbf{e}\mathbf{I}_{\theta\theta}+\nabla\mathbf{N}_{w\theta})^T\mathbf{D_s}(\mathbf{e}\mathbf{I}_{\theta\theta}+\nabla\mathbf{N}_{w\theta})dA$$

$$\mathbf{K}_{\mathbf{S}w\theta}=\int_A(\mathbf{e}\mathbf{I}_{\theta\theta}+\nabla\mathbf{N}_{w\theta})^T\mathbf{D_s}(\nabla\mathbf{I}_{ww})dA$$

$$\mathbf{K}_{\mathbf{S}wb}=\int_A(\nabla N_{wb})^T\mathbf{D_s}(\nabla\mathbf{I}_{ww})dA$$

$$\mathbf{K}_{\mathbf{S}b\theta}=\int_A(\nabla N_{wb})^T\mathbf{D_s}(\mathbf{e}\mathbf{I}_{\theta\theta}+\nabla\mathbf{N}_{w\theta})dA$$

where $\mathbf{L}$, ∇ are the differential operators from (2) and (3) acting on the interpolation functions in (17) and (16), respectively, while $\mathbf{e}$ is the unit transformation matrix given in (2).

4. Test examples

In all the examples to follow the elements presented are denoted as *Q4-U2* for the four-node element, *Q9-U3* for the nine-node element and *Q16-U4* for the sixteen-node element. The results are compared to the mixed-type element of Auricchio and Taylor [3] denoted as *Q4-LIM* and to the hybrid-type element of de Miranda and Ubertini [9] denoted as *9βQ4*.

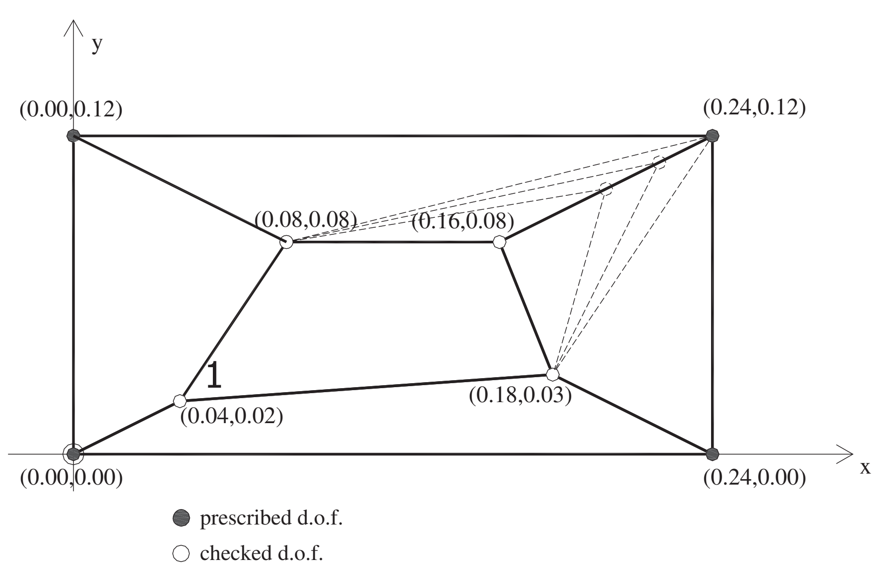

Fig. 7. Patch for consistency assessment of four-node elements.

4.1. Patch test

Consistency of the interpolation functions for the developed elements is tested for the constant strain and stress conditions on the patch example with five irregular elements, covering a rectangular domain of a plate as shown in Fig. 7 [31,32]. The displacements and rotations for the four internal nodes within the patch are tested given the specific displacements and rotations for the four external nodes. The plate properties are chosen as $E=10^5$, $\nu=0.25$, $k=\frac{5}{6}$ and two values of the plate thickness are considered: $h=1.0$ and 0.01, corresponding to a thick and a thin plate, respectively.

Two strain–stress states are tested:

- Constant bending strain/stress state (zero shear deformation [32])

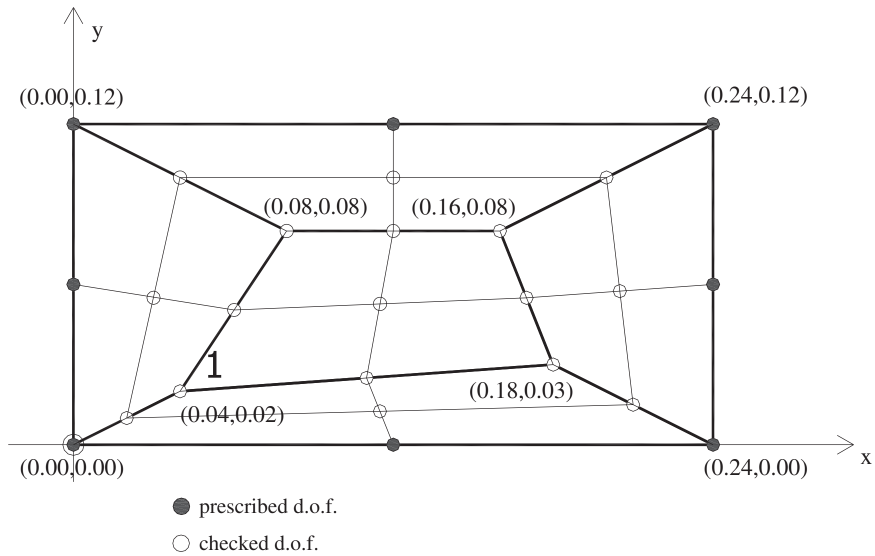

Fig. 8. Patch for consistency assessment of nine-node elements.

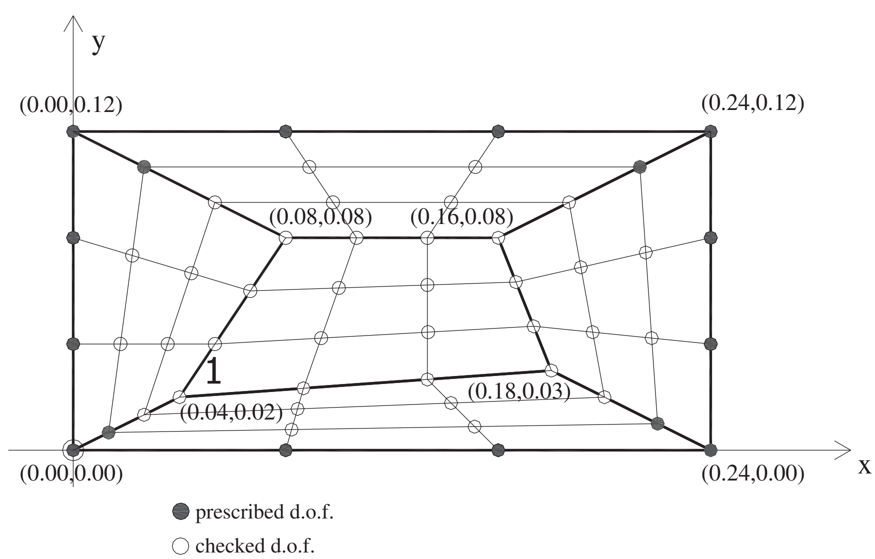

Fig. 9. Patch for consistency assessment of sixteen-node elements.

Table 1
The patch test results for three proposed elements (control deformation at point 1: w_1).

Elements	*Patch test for zero shear*			*Patch test for non-zero constant shear*		
	h=1.0	*h=0.01*	*Result*	*h=1.0*	*h=0.01*	*Result*
Q4-U2	0.5414000	0.5414000	Pass	−0.2456171	−0.000017896	Fail
Q9-U3	0.5414000	0.5414000	Pass	−0.2450933	0.000215467	Pass
Q16-U4	0.5414000	0.5414000	Pass	−0.2450933	0.000215467	Pass
Analytical solution	0.5414	0.5414		−0.245093333	0.000215467	

Table 2
Clamped square plate: displacement and moment at the centre with regular meshes, $L/h=10$.

Element mesh	*Q4-U2*		*Q9-U3*		*Q16-U4*	
	w^*	M^*	w^*	M^*	w^*	M^*
1×1	0.02679	0.0	0.15059	3.40254	0.14974	2.08359
2×2	0.11920	2.02221	0.15046	2.45416	0.15041	2.30177
4×4	0.14361	2.25778	0.15044	2.34636	0.15046	2.31802
8×8	0.14876	2.30471	0.15046	2.32618	0.15046	2.31966
16×16	0.15004	2.31616	0.15046	2.32152		
32×32	0.15036	2.31903	0.15046	2.32037		
64×64	0.15044	2.31975				
Ref. sol. [11]	0.1499	2.31	0.1499	2.31	0.1499	2.31

Element mesh	*Q4-LIM* [3]		*9βQ4* [9]	
	w^*	M^*	w^*	M^*
1×1				
2×2	0.14211	1.8108	0.1625190	2.83817
4×4	0.14858	2.1968	0.1534432	2.44825
8×8	0.14997	2.2889	0.1511805	2.35119
16×16	0.15034	2.3122	0.1506379	2.32770
32×32	0.15043	2.3180	0.1505061	2.32191
64×64				
Ref. sol. [11]	0.1499	2.31	0.1499	2.31

Table 3
Clamped square plate: displacement and moment at the centre with regular meshes, $L/h=1000$.

Element mesh	*Q4-U2 (G.p.3x3)*		*Q9-U3 (G.p.4x4)*		*Q16-U4 (G.p.5x5)*	
	w^*	M^*	w^*	M^*	w^*	M^*
1×1	0.0000027		0.00027	0.00746	0.13241	3.70328
2×2	0.00013	−0.0001	0.09918	2.03484	0.12646	2.40533
4×4	0.00469	0.10731	0.12112	2.24000	0.12653	2.29613
8×8	0.05988	1.18496	0.12621	2.29083	0.12653	2.29039
16×16	0.11899	2.17415	0.12653	2.29179		
32×32	0.12600	2.28275	0.12653	2.29086		
64×64	0.12648	2.28988				
Ref. sol. [11]	0.126532	2.29051	0.126532	2.29051	0.126532	2.29051

Element mesh	*Q4-U2 (G.p.2x2)*		*Q9-U3 (G.p.3x3)*		*Q16-U4 (G.p.4x4)*	
	w^*	M^*	w^*	M^*	w^*	M^*
1×1	0.0000027		0.00060	0.01432	0.13229	3.46904
2×2	0.00017	−0.0004	0.09832	1.90152	0.12627	2.24644
4×4	0.01053	0.27246	0.12163	2.23799	0.12653	2.28636
8×8	0.09571	1.98924	0.12629	2.28926	0.12653	2.28986
16×16	0.12406	2.26656	0.12653	2.29105		
32×32	0.12634	2.28849	0.12653	2.29066		
64×64	0.12650	2.29016				
Ref. sol. [11]	0.126532	2.29051	0.126532	2.29051	0.126532	2.29051

Element mesh	*Q4-LIM* [3]		*9βQ4* [9]	
	w^*	M^*	w^*	M^*
1×1				
2×2	0.11469	1.7311	0.13766768	2.745544
4×4	0.12362	2.1629	0.12938531	2.423885
8×8	0.12584	2.2590	0.12725036	2.323949
16×16	0.12637	2.2827	0.12671406	2.298876
32×32	0.12649	2.2886	0.12657946	2.292605
64×64				
Ref. sol. [11]	0.126532	2.29051	0.126532	2.29051

Displacements and rotations are expressed, respectively, by

$$w=(1+x+2y+x^2+xy+y^2)/2, \quad \theta_x=(2+x+2y)/2,$$
$$\theta_y=-(1+2x+y)/2,$$

with no body forces.

The exact displacements and rotations at the internal nodes and the exact strains/stresses at every integration point are expected. The moments are constant $M_x=M_y=-11111.11\,h^3$, $M_{xy}=-33333.33\,h^3$ and the shear forces vanish ($S_x=S_y=0$).

- Constant shear strain/stress state (non-zero constant shear deformation [32])

  Displacements and rotations are expressed, respectively, by

$$w=-\frac{h^2}{5(1-\nu)}(14x+18y)+x^3+2y^3+3x^2y+4xy^2,$$
$$\theta_x=3x^2+8xy+6y^2$$
$$\theta_y=-(3x^2+6xy+4y^2).$$

The exact displacements and rotations at the internal nodes and the exact strains/stresses at every integration point are expected again. The shear forces are constant $S_x=-124400.0\,h^3$ and $S_y=-160000.0\,h^3$ in every Gauss point and the moments are linearly distributed according to

$$M_x=-\frac{Eh^3}{12(1-\nu^2)}[x(6+8\nu)+y(6+12\nu)],$$
$$M_y=-\frac{Eh^3}{12(1-\nu^2)}[x(8+6\nu)+y(12+6\nu)]$$
$$\text{and} \quad M_{xy}=-\frac{Eh^3}{12(1-\nu^2)}\frac{1-\nu}{2}(12x+16y).$$

The four-node element is tested on the patch given in Fig. 7 for constant bending state. For the values of the displacements and rotations at the external nodes calculated from the above data, the displacements and rotations at the internal nodes as well as the bending and torsional moments and the shear forces at the integration points are calculated and correspond exactly to the analytical results given above. The results are not affected if the internal nodes are defined at a different set of co-ordinates including the case in which one of the internal nodes corresponds with the upper right-hand corner of the patch as shown in Fig. 7. Effectively, the element naturally degenerates to a triangular element, which is also an observation made in [26].

The nine-node element is tested on the same patch examples (the mesh is given in Fig. 8). Only the displacements and rotations at the boundary nodes are given (8 displacements and 16 rotations). All the other nodal displacements and rotations are to be calculated and they are calculated exactly for both the constant bending and the constant shear tests. The moments and shear forces at the integration points are again exact.

The same patch tests are also successfully performed by five sixteen-node elements, where 48 parameters for the degrees of freedom are prescribed and 108 others are checked out (Fig. 9).

The results of the patch tests for all three proposed elements are given in Table 1 for the control displacement at node 1. All elements can pass the patch test for zero shear deformation and only *Q4-U2* fails the test for non-zero constant shear.

4.2. Clamped square plate

In this example, a quadratic plate with clamped edges is considered. Only one quarter of the plate is modelled with symmetric boundary conditions imposed on the symmetry lines. Two ratios of span versus thickness are analysed, $L/h=10$ representing a relatively thick plate and $L/h=1000$ representing its thin counterpart. The loading on the plate is uniformly distributed of magnitude $q=1$. The plate material properties are $E=10.92$ and $\nu=0.3$.

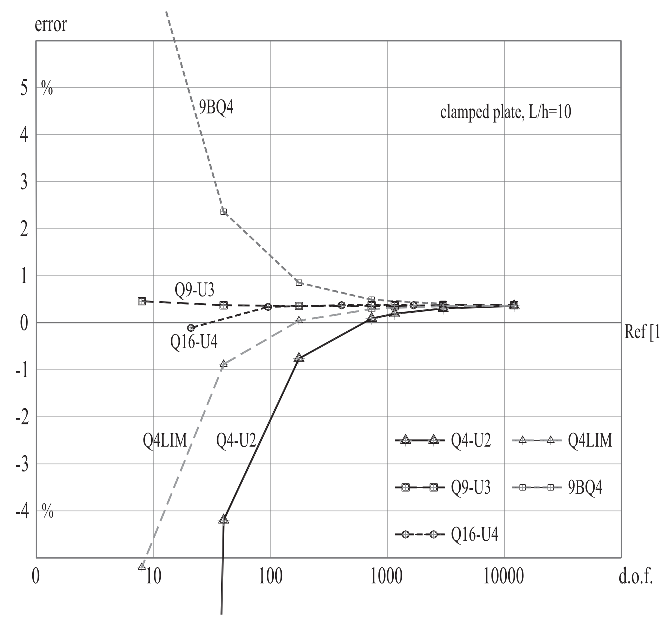

Fig. 11. Convergence of the transverse displacement error at the centre on regular meshes for clamped plate $L/h=10$.

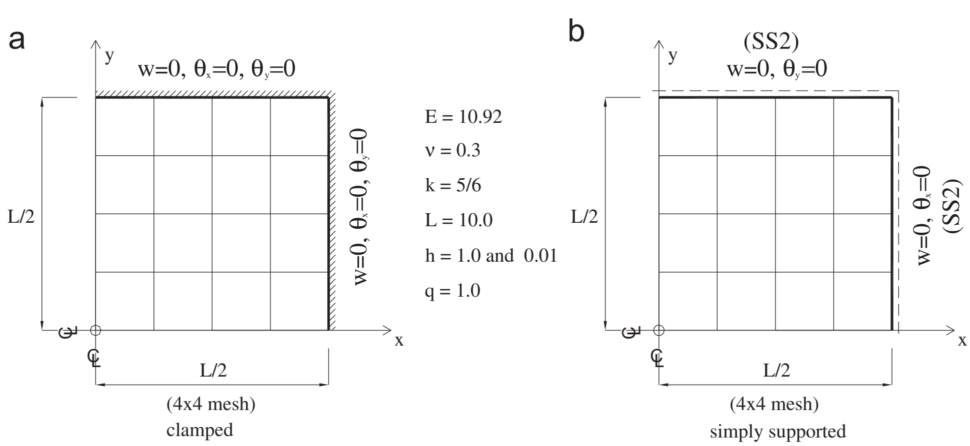

Fig. 10. A quarter of the square plate under uniform load (16-element mesh).

Numerical results are given in Tables 2 and 3 and compared to the elements presented in [3,9] based on the mixed approach and with the reference solutions taken from [11]. The dimensionless results $w^*=w/(qL^4/(100D))$ and $M^*=M/(qL^2/100)$, where $D=Eh^3/(12(1-\nu^2))$ and L is the plate span, given in these tables are related to the central displacement of the plate and the bending moment at the integration point nearest to the centre of the plate. The number of elements per mesh in these tables relates to one quarter of the structure as shown in Fig. 10a. for the mesh of 4×4 elements.

Convergence of the displacement error is presented in Fig. 11, with respect to the number of degrees of freedom in chosen element meshes (in logarithmic scale). Zero error value corresponds to the referent solution taken from [3,11]. Best convergence with respect to the number of degrees of freedom can be observed in elements with higher-order linked interpolation and it may be concluded that for the thick clamped plate the present elements converge competitively for a comparable number of degrees of freedom.

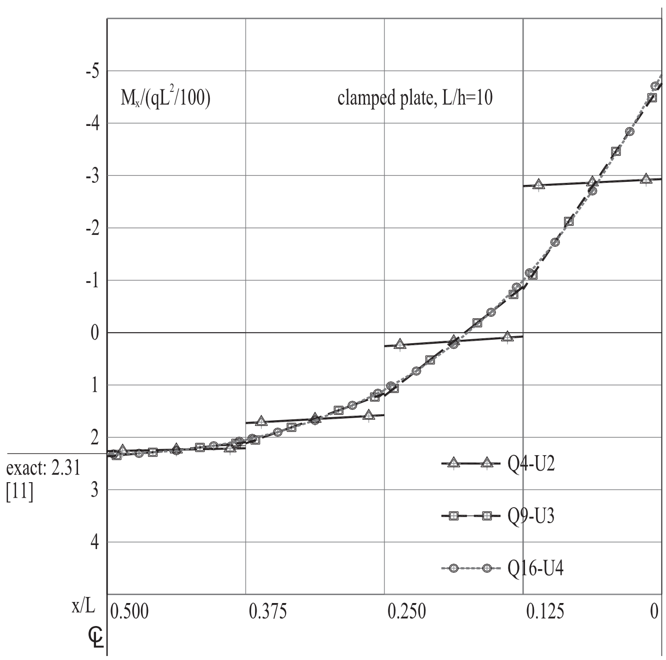

Fig. 12. Moment M_x distribution along element's Gauss points closest to the x-axis on the 4×4 regular mesh for the clamped plate with $L/h=10$.

In Fig. 12, the M_x moment distribution along the x-axis is shown (actually at the Gauss points closest to the axis), beginning from the centre point of the plate (origin of the co-ordinate system of the mesh). These results are the same as the results for the moment M_y along the y-direction. For *Q4-U2* element, the moment is distributed linearly across the element, owing to its dependence on the curvatures in both directions for any non-zero value of the Possion coefficient (4). For $\nu=0$ this moment would be constant as in the Timoshenko beam. For higher-order elements, the moment distribution is accordingly described by higher-order polynomials, and the results converge towards the exact distribution fast. Similar observations may be made for the shear-stress resultant S_x distribution along the x-axis (not shown), only that for the lower-order element *Q4-U2* the linear distribution of S_x is now due to the internal bubble interpolation function in the second term of (9) without which it would be constant.

For the thin plate case shown in Table 3, the elements *Q4-U2* and *Q9-U3* obviously suffer from shear locking when the meshes are coarse, but they still converge to the correct result competitively fast, in particular the higher-order elements *Q9-U3* and *Q16-U4*.

A comparison is also made between full integration rule for the strain energy, i.e. 3 by 3 integration points for quadratic interpolation (*Q4-U2*), 4 by 4 integration for cubic interpolation (*Q9-U3*) and 5 by 5 integration for quartic interpolation (*Q16-U4*), and the reduced integration on the respective elements.

The reduced integration in the middle part of Table 3 shows some improvement in convergence for low order elements and coarse meshes, but has no importance for higher order elements and dense meshes.

4.3. Simply supported square plate

In this example, the same quadratic plate as before is considered, but this time with the simply supported edges of the type SS2 (displacements and rotations around the normal to the edge

Table 4
Simply supported square plate (SS2) under uniformly distributed load: displacement and moment at the centre with regular meshes, $L/h=10$.

Element mesh	*Q4-U2*		*Q9-U3*		*Q16-U4*	
	w^*	M^*	w^*	M^*	w^*	M^*
1×1	0.26102	2.88202	0.42983	5.33564	0.42717	4.66623
2×2	0.41163	4.66892	0.42749	4.86404	0.42728	4.77762
4×4	0.42448	4.77207	0.42730	4.80320	0.42728	4.78712
8×8	0.42664	4.78515	0.42729	4.79203	0.42728	4.78833
16×16	0.42713	4.78781	0.42728	4.78947		
32×32	0.42725	4.78843	0.42728	4.78885		
64×64	0.42727	4.78859				
Navier series [11]	0.427284	4.78863	0.427284	4.78863	0.427284	4.78863

Element mesh	*Q4-LIM* [3]		*9βQ4* [9]	
	w^*	M^*	w^*	M^*
1×1				
2×2	0.42626	4.4686	0.4286943	5.264135
4×4	0.42720	4.7099	0.4276333	4.905958
8×8	0.42727	4.7690	0.4273690	4.817645
16×16	0.42728	4.7837	0.4273052	4.795864
32×32	0.42728	4.7874	0.4272895	4.790443
64×64				
Navier series [11]	0.427284	4.78863	0.427284	4.78863

Table 5
Simply supported square plate (SS2) under uniformly distributed load: displacement and moment at the centre with regular meshes, $L/h=1000$.

Element mesh	*Q4-U2*		*Q9-U3*		*Q16-U4*	
	w^*	M^*	w^*	M^*	w^*	M^*
1 × 1	0.0000008	0.00093	0.35527	3.67992	0.41220	5.49186
2 × 2	0.0031093	0.03842	0.39807	4.66131	0.40647	4.85587
4 × 4	0.055621	0.68507	0.40475	4.76923	0.40624	4.79124
8 × 8	0.29658	3.54861	0.40615	4.78990	0.40624	4.78843
16 × 16	0.39706	4.68543	0.40624	4.78943		
32 × 32	0.40562	4.78188	0.40624	4.78884		
64 × 64	0.40619	4.78764				
Navier series [11]	0.406237	4.78863	0.406237	4.78863	0.406237	4.78863

Element mesh	*Q4-LIM* [3]		*9βQ4* [9]	
	w^*	M^*	w^*	M^*
1 × 1	0.37646	2.018		
2 × 2	0.40365	4.119	0.4063653	5.241563
4 × 4	0.40586	4.623	0.4063062	4.904153
8 × 8	0.40616	4.747	0.4062559	4.817513
16 × 16	0.40622	4.778	0.4062421	4.795855
32 × 32	0.40623	4.786	0.4062386	4.790442
64 × 64	0.40624	4.788		
Navier series [11]	0.406237	4.78863	0.406237	4.78863

set to zero) as shown in Fig. 10b. The same elements as before are tested and the results are given in Tables 4 and 5 for the thick and the thin plate, respectively, compared again to the elements presented in [3,9].

As before, the dimensionless results $w^*=w/(qL^4/(100D))$ and $M^*=M/(qL^2/100)$ given in these tables are related to the central displacement of the plate and the bending moment at the integration point nearest to the centre of the plate. The number of elements per mesh in these tables relates to one quarter of the structure.

For the thick plate case it can be concluded that elements *Q4-U2* and *Q9-U3* converge a little slower, but element *Q16-U4* shows remarkable accuracy even for a very coarse mesh.

For the thin plate case element *Q4-U2* still suffers from shear locking, but elements *Q9-U3* and *Q16-U4* again show very good convergence rate.

4.4. Simply supported skew plate

In this example, the rhombic plate is considered with the simply supported edges (this time, however, with the so-called soft type SS1—only the edge displacements are set to zero as argued in [33]) to test performance of the elements when they depart from the rectangular shape, but remain paralleloid. The problem geometry and material properties are given in Fig. 13, where an example of a 64-element mesh is also shown.

The same three elements as before are tested and the results are given in Tables 6 and 7 for the thick and the thin plate, respectively. The dimensionless results $w^*=w/(qL^4/(10^4D))$, $M^*_{11}=M_{11}/(qL^2/100)$ and $M^*_{22}=M_{22}/(qL^2/100)$ are related to the central displacement of the plate and the principal bending moments in diagonal directions at the integration point nearest to the centre of the plate.

In contrast to the earlier examples, it must be noted that here the new displacement-based elements perform worse than the elements given in [3,9], both for the thick and the thin plate examples.

The tested example has two orthogonal axes of symmetry, A–C–B and D–C–E, and only one triangular quarter may be taken for analysis [29,34]. Since there is a singularity in the moment field at the obtuse vertex, this test example is a difficult one. Even more, the analytical solution reveals that moments in the principal directions near the obtuse vertex have opposite signs.

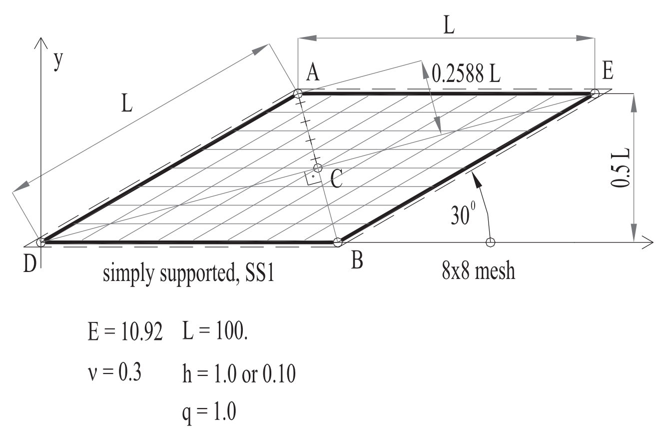

Fig. 13. A simply supported (SS1) skew plate under uniform load.

The moment results for direction ''A–C–B'' (not shown) converge towards the exact solution satisfactorily, but the moment for direction ''D–C–E'' in Fig. 14 for the Gauss points on the diagonal from vertex A to the central point C of the plate shows that this family of elements struggles to follow the exact moment distribution near the singularity point.

4.5. Simply supported circular plate

As our last example, the circular plate with the simply supported edges (type SS1) is analysed. The element mesh is obviously irregular with non-parallel element sides so the influence of such irregularity is observed on the behaviour of our three elements.

The results are given in Tables 8 and 9 for the thick and the thin plate, respectively. The problem geometry and material properties are given in Fig. 15 (only one quarter of the plate is analysed), where an example of a 12-element mesh is also shown.

Table 6
Simply supported skew plate (SS1): displacement and moment at the centre with regular meshes, $L/h=100$.

Element mesh	*Q4-U2*			*Q9-U3*			*Q16-U4*		
	w^*	M^*_{22}	M^*_{11}	w^*	M^*_{22}	M^*_{11}	w^*	M^*_{22}	M^*_{11}
2×2	0.06153	0.1349	0.3763	0.21493	0.4860	1.0536	0.28406	0.8404	1.5335
4×4	0.16287	0.3659	0.9226	0.32974	0.8227	1.6486	0.37778	0.9642	1.8310
8×8	0.29165	0.6870	1.4858	0.38719	1.0083	1.8508	0.40497	1.0681	1.8962
16×16	0.37449	0.9470	1.7959	0.40904	1.0890	1.9094	0.41774	1.1172	1.9345
24×24	0.39633	1.0348	1.8690	0.41554	1.1115	1.9279			
32×32	0.40536	1.0696	1.8890						
48×48	0.41326	1.1028	1.9213						
Ref. [35]	0.423			0.423			0.423		

Element mesh	*Q4-LIM* [3]			*9βQ4* [9]		
	w^*	M^*_{22}	M^*_{11}	w^*	M^*_{22}	M^*_{11}
2×2	0.55685	0.5400	1.1805			
4×4	0.43840	0.8898	1.8141	0.502900	1.354215	2.054527
8×8	0.42499	1.0555	1.9181	0.443176	1.082957	1.956494
16×16	0.42124	1.1072	1.9355	0.432211	1.149921	1.966940
24×24						
32×32	0.42178	1.1263	1.9440	0.426964	1.148682	1.959293
48×48						
Ref. [35]	0.423			0.423		

Table 7
Simply supported skew plate (SS1): displacement and moment at the centre with regular meshes, $L/h=1000$.

Element mesh	*Q4-U2*			*Q9-U3*			*Q16-U4*		
	w^*	M^*_{22}	M^*_{11}	w^*	M^*_{22}	M^*_{11}	w^*	M^*_{22}	M^*_{11}
2×2	0.00087	0.0018	0.0048	0.15198	0.2596	0.5436	0.24947	0.7742	1.4298
4×4	0.00940	0.0222	0.0604	0.24245	0.5181	1.0542	0.32983	0.8966	1.7738
8×8	0.08101	0.1991	0.5320	0.31048	0.7569	1.5423	0.35493	0.9036	1.7595
16×16	0.20304	0.4738	1.1403	0.35670	0.9010	1.7574	0.37775	0.9730	1.8191
24×24	0.27309	0.6451	1.4369	0.37401	0.9595	1.8097			
32×32	0.31365	0.7544	1.5910						
48×48	0.35353	0.8802	1.7386						
Ref. [36]	0.4080	1.08	1.91	0.4080	1.08	1.91	0.4080	1.08	1.91

Element mesh	*Q4-LIM* [3]			*9βQ4* [9]		
	w^*	M^*_{22}	M^*_{11}	w^*	M^*_{22}	M^*_{11}
2×2	0.55530	0.5376	1.1809			
4×4	0.43670	0.8864	1.8052	0.501994	1.352235	2.056188
8×8	0.42064	1.0494	1.9105	0.442198	1.079937	1.955570
16×16	0.41560	1.0916	1.9203	0.430832	1.149342	1.964564
24×24						
32×32	0.41363	1.1008	1.9209	0.424505	1.143222	1.953153
48×48						
Ref. [36]	0.4080	1.08	1.91	0.4080	1.08	1.91

Again, here the displacement-based elements presented converge very quickly towards the exact solution, in particular the nine-node *Q9-U3* element and the sixteen-node *Q16-U4* element, which provides better results than the other elements for the comparable number of the degrees of freedom.

5. Conclusions

In this work, the use of purely displacement-based linked interpolation in the design of Mindlin plate finite elements is presented and numerically assessed. We have specifically considered quadrilateral four-, nine- and sixteen-node plate elements, for which the shear strain condition of a certain order imposed on the element edges leads to the so-called linked interpolation for the displacement field whereby the nodal rotations around the normal to the element edges also contribute to the element out-of-plane displacements.

In contrast to the mixed-type approaches, here it has been confirmed that, for the lowest-order element, an additional internal degree of freedom is required in order to satisfy the standard patch tests. The elements developed in this way are capable of reproducing the exact analytical result for the case of cylindrical bending of certain order (quadratic for the four-node

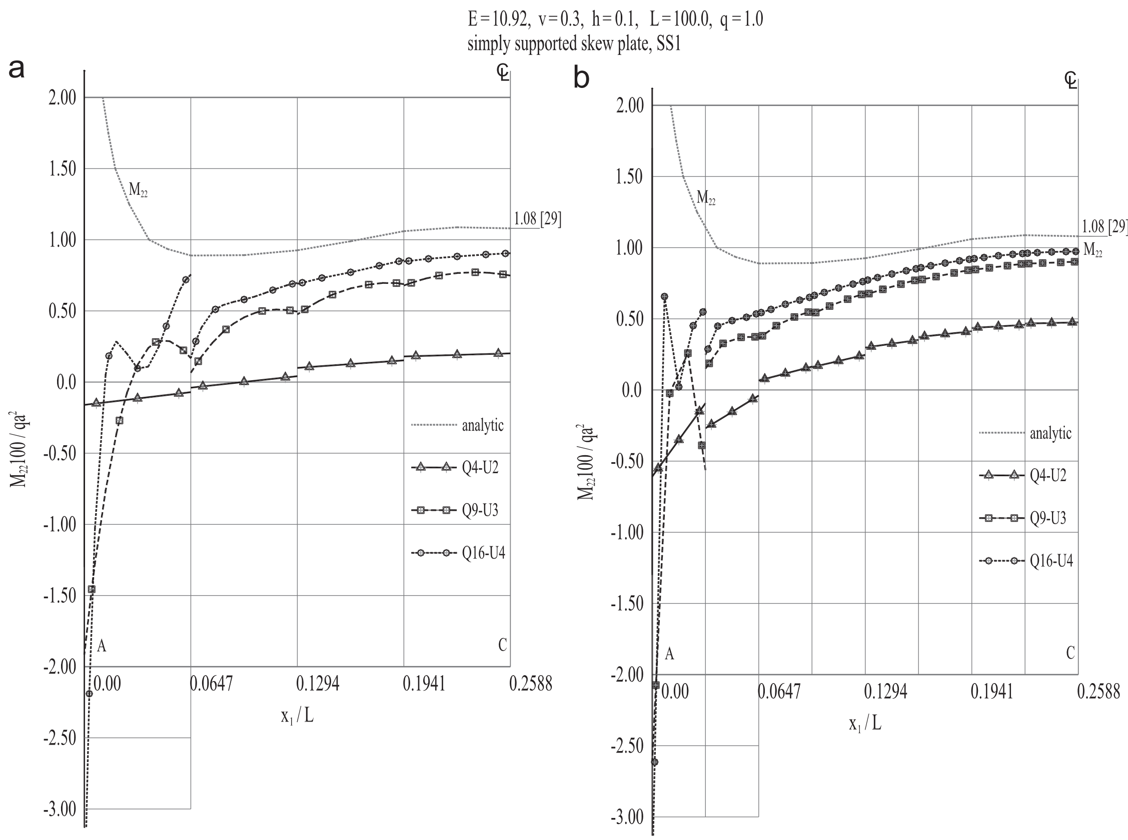

Fig. 14. Simply supported skew plate under uniform load—principal moment in D–C–E direction (M_{22}) distribution in Gauss points along diagonal A–C using: (a) 8×8 element mesh and (b) 16×16 element mesh for the whole plate.

Table 8
Simply supported circular plate (SS1): displacement and moment at the centre, $R/h=5$ ($h=1.0$).

Element mesh	*Q4-U2*		*Q9-U3*		*Q16-U4*	
	w_c^*	M_c^*	w_c^*	M_c^*	w_c^*	M_c^*
3	0.410450	4.9346	0.415679	5.2185	0.416237	5.1547
12	0.414462	5.1251	0.415977	5.1831	0.416028	5.1552
48	0.415615	5.1494	0.415992	5.1641		
192	0.415893	5.1546				
768						
Ref. [9]	0.415994	5.1563	0.415994	5.1563	0.415994	5.1563

Element mesh	*Q4-LIM* [3]		*9βQ4* [9]	
	w_c^*	M_c^*	w_c^*	M_c^*
3	0.42191	4.8010	0.2812290	5.11686
6	0.41760	5.0682		
12	0.41641	5.1337	0.4133307	5.16833
24	0.41610	5.1505		
48	0.41602	5.1548	0.4153994	5.16188
192			0.4158536	5.15782
768			0.4159633	5.15669
Ref. [9]	0.415994	5.1563	0.415994	5.1563

With: $w^*=w/(16\,qR^4/(100D))$, $M_x=M_y=M_c$, $M_c^*=M_c/(4\,qR^2)$ (at closest Gauss point), $D=Eh^3/(12(1-\nu^2))$ and R is a plate radius.

elements, cubic for the nine-node elements and so on), but still suffer from the shear-locking effect for very coarse meshes and the lowest-order element types.

However, these elements perform competitively for a number of standard benchmark tests as the finite-element mesh is refined, one notable exception being the skewed plate, for which the presented elements do not perform so well. Otherwise, the nine- and the sixteen-node elements, in general, are clearly successful when compared to lower-order elements for the problems with the same total number of the degrees of freedom.

Table 9
Simply supported circular plate (SS1): displacement and moment at the centre, $R/h=50$ ($h=0.1$).

Element mesh	*Q4-U2*		*Q9-U3*		*Q16-U4*	
	w_c^*	M_c^*	w_c^*	M_c^*	w_c^*	M_c^*
3	0.3486007	3.85988	0.3904531	5.10265	0.397474	5.1484
12	0.3828163	4.82198	0.3981520	5.17865	0.398265	5.1553
48	0.3968067	5.12375	0.3982781	5.16337		
192	0.3981513	5.15283				
768						
Ref. [9]	0.398315	5.1563	0.398315	5.1563	0.398315	5.1563

Element mesh	*Q4-LIM* [3]		*9βQ4* [9]	
	w_c^*	M_c^*	w_c^*	M_c^*
3	0.40576	4.7980	0.2692074	5.10642
6	0.40027	5.0670		
12	0.39881	5.1335	0.3959145	5.14593
24	0.39844	5.1505		
48	0.39835	5.1548	0.3977919	5.16070
192			0.3981935	5.15773
768			0.3982894	5.15668
Ref. [9]	0.398315	5.1563	0.398315	5.1563

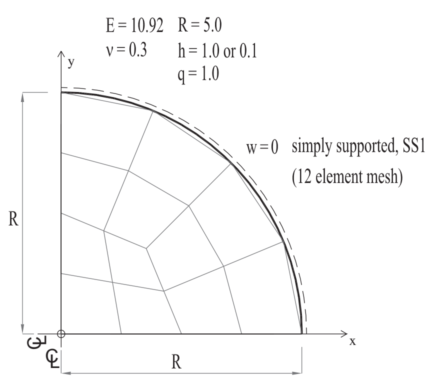

Fig. 15. A simply supported (SS1) skew plate under uniform load.

Acknowledgement

The results shown here have been obtained within the Scientific Project no. 114-0000000-3025: "Improved accuracy in non-linear beam elements with finite 3D rotations" financially supported by the Ministry of Science, Education and Sports of the Republic of Croatia.

References

[1] F. Auricchio, R.L. Taylor, A new family of quadrilateral thick plate finite elements based on linked interpolation, Report no. UCB/SEMM-93/10, University of California at Berkeley, Department of Civil Engineering, Berkeley, 1993.
[2] A. Ibrahimbegović, Quadrilateral finite-elements for analysis of thick and thin plates, Computer Methods in Applied Mechanics and Engineering 110 (1993) 195–209.
[3] F. Auricchio, R.L. Taylor, A shear deformable plate element with an exact thin limit, Computer Methods in Applied Mechanics and Engineering 118 (1994) 393–412.
[4] C. Chinosi, F. Lovadina, Numerical analysis of some mixed finite element methods for Reissner–Mindlin plate, Computational Mechanics 16 (1995) 36–44.
[5] F. Auricchio, C. Lovadina, Analysis of kinematic linked interpolation methods for Reissner–Mindlin plate problem, Computer Methods in Applied Mechanics and Engineering 190 (2001) 2465–2482.
[6] R.L. Taylor, S. Govindjee, A quadratic linked plate element with an exact thin plate limit, Report no. UCB/SEMM-2002/10, University of California at Berkeley, Department of Civil and Environmental Engineering, Berkeley, 2002.
[7] O.C. Zienkiewicz, R.L. Taylor, The Finite Element Method for Solid and Structural Mechanics, Elsevier Butterworth-Heinemann, Oxford, 2005.
[8] Y.J. Liu, H.R. Riggs, The MIN-N family of pure-displacement, triangular, Mindlin plate elements, Structural Engineering and Mechanics 19 (2005) 297–320.
[9] S. de Miranda, F. Ubertini, A simple hybrid stress element for shear deformable plates, International Journal for Numerical Methods in Engineering 65 (2006) 808–833.
[10] M.A. Crisfield, Finite Elements and Solution Procedures for Structural Analysis, Pineridge Press, Swansea, 1986.
[11] O.C. Zienkiewicz, Z. Xu, L.F. Zeng, A. Samuelsson, N.E. Wiberg, Linked interpolation for Reissner–Mindlin plate elements: Part I—A simple quadrilateral, International Journal for Numerical Methods in Engineering 36 (1993) 3043–3056.
[12] R.L. Taylor, F. Auricchio, Linked interpolation for Reissner–Mindlin plate elements: Part II—A simple triangle, International Journal for Numerical Methods in Engineering 36 (1993) 3057–3066.
[13] Z. Xu, O.C. Zienkiewicz, L.F. Zeng, Linked interpolation for Reissner–Mindlin plate elements: Part III—An alternative quadrilateral, International Journal for Numerical Methods in Engineering 37 (1994) 1437–1443.
[14] W.J. Chen, Y.K. Cheung, Refined quadrilateral element based on Mindlin/Reissner plate theory, International Journal for Numerical Methods in Engineering 47 (2000) 605–627.
[15] W.J. Chen, Y.K. Cheung, Refined 9-dof triangular Mindlin plate elements, International Journal for Numerical Methods in Engineering 51 (2001) 1259–1281.
[16] W.J. Chen, Y.K. Cheung, Refined discrete quadrilateral degenerated shell element by using Timoshenko's beam function, International Journal for Numerical Methods in Engineering 63 (2005) 1203–1227.
[17] A. Tessler, S.B. Dong, On a hierarchy of conforming Timoshenko beam elements, Computers and Structures 14 (1981) 335–344.
[18] G. Jelenić, E. Papa, Exact solution of 3D Timoshenko beam problem using linked interpolation of arbitrary order, Archive of Applied Mechanics 18 (2011) 171–183.
[19] J. Przemieniecki, Theory of Matrix Structural Analysis, McGraw-Hill, New York, 1968.
[20] J. Rakowski, The interpretation of the shear locking in beam elements, Computers and Structures 37 (1990) 769–776.
[21] L. Yunhua, Explanation and elimination of shear locking and membrane locking with field consistence approach, Computer Methods in Applied Mechanics and Engineering 162 (1998) 249–269.
[22] J.N. Reddy, On locking-free shear deformable beam finite elements, Computer Methods in Applied Mechanics and Engineering 149 (1997) 113–132.
[23] S. Mukherjee, J.N. Reddy, C.S. Krishnamoorthy, Convergence properties and derivative extraction of the superconvergent Timoshenko beam finite element, Computer Methods in Applied Mechanics and Engineering 190 (2001) 3475–3500.
[24] A. Tessler, T.J.R. Hughes, An improved treatment of transverse shear in the Mindlin-type four node quadrilateral element, Computer Methods in Applied Mechanics and Engineering 39 (1983) 311–335.
[25] J.C. Simo, M.S. Rifai, A class of mixed assumed-strain methods and the method of incompatible modes, International Journal for Numerical Methods in Engineering 29 (1990) 1595–1638.
[26] F. Kikuchi, K. Ishii, An improved 4-node quadrilateral plate bending element of the Reissner–Mindlin type, Computer Methods in Applied Mechanics and Engineering 195 (2006) 3448–3460.

[27] F. Auricchio, R.L. Taylor, A triangular thick plate finite element with an exact thin limit, Finite Elements in Analysis and Design 19 (1995) 57–68.
[28] K.-J. Bathe, Finite Element Procedures, Prentice Hall, New Jersey, 1989.
[29] T.J.R. Hughes, The Finite Element Method. Linear Static and Dynamic Finite Element Analysis, Dover Publications inc., Mineola, New York, 2000.
[30] O.C. Zienkiewicz, R.L. Taylor, J.Z. Zhu, The Finite Element Method. Its Basis and Fundamentals, Elsevier Butterworth-Heinemann, Oxford, 2005.
[31] W.J. Chen, Enhanced patch test of finite element methods, Science in China, Series G: Physics, Mechanics & Astronomy 49 (2006) 213–227.
[32] W.J. Chen, J.Z. Wang, J. Zhao, Functions for patch test in finite element analysis of the Mindlin plate and the thin cylindrical shell, Science in China, Series G: Physics, Mechanics & Astronomy 52 (2009) 762–767.
[33] I. Babuška, T. Scapolla, Benchmark computation and performance evaluation for a rhombic plate bending problem, International Journal for Numerical Methods in Engineering 28 (1989) 155–179.
[34] T.J.R. Hughes, T.E. Tezduyar, Finite elements based upon Mindlin plate theory with particular reference to the four-node bilinear isoparametric element, Journal of Applied Mechanics 48 (1981) 587–596.
[35] Z. Zhu, A thick-thin triangular plate element, International Journal for Numerical Methods in Engineering 33 (1992) 963–973.
[36] L.S.D. Morley, Bending of simply supported rhombic plate under uniform normal loading, Quarterly Journal of Mechanics and Applied Mathematics 15 (1962) 413–426.